

SCIseg: Automatic Segmentation of T2-weighted Intramedullary Lesions in Spinal Cord Injury

Enamundram Naga Karthik, MSc*^{†1,2}, Jan Valosek, PhD*^{1,2,3,4}, Andrew C. Smith, PT, DPT, PhD⁵, Dario Pfyffer, PhD^{6,7}, Simon Schading-Sassenhausen, MSc⁶, Lynn Farner, MSc⁶, Kenneth A. Weber II, DC, PhD⁷, Patrick Freund, MD, PhD^{6,8}, Julien Cohen-Adad, PhD^{1,2,9,10}

*Shared co-first authorship - authors contributed equally

[†]Corresponding author (email: naga-karthik.enamundram@polymtl.ca)

1. NeuroPoly Lab, Institute of Biomedical Engineering, Polytechnique Montreal, Montreal, QC, Canada
2. Mila - Quebec AI Institute, Montreal, QC, Canada
3. Department of Neurosurgery, Faculty of Medicine and Dentistry, Palacký University Olomouc, Olomouc, Czechia
4. Department of Neurology, Faculty of Medicine and Dentistry, Palacký University Olomouc, Olomouc, Czechia
5. Department of Physical Medicine and Rehabilitation Physical Therapy Program, University of Colorado School of Medicine, Aurora, Colorado, USA
6. Spinal Cord Injury Center, Balgrist University Hospital, University of Zürich, Zürich, Switzerland
7. Department of Anesthesiology, Perioperative and Pain Medicine, Stanford University School of Medicine, Stanford, California, USA
8. Department of Neurophysics, Max Planck Institute for Human Cognitive and Brain Sciences, Leipzig, Germany
9. Functional Neuroimaging Unit, CRIUGM, Université de Montréal, Montreal, QC, Canada
10. Centre de Recherche du CHU Sainte-Justine, Université de Montréal, Montreal, QC, Canada

Summary

Automatic segmentation of the spinal cord and T2-weighted lesions in spinal cord injury on MRI scans across different treatment strategies, lesion etiologies, sites, scanner manufacturers, and heterogeneous image resolutions.

Key Results

- An open-source, automatic method, *SCIseg*, was trained and evaluated on a dataset of 191 spinal cord injury patients from three sites for the segmentation of the spinal cord and T2-weighted lesions.
- *SCIseg* generalizes across traumatic and non-traumatic lesions, scanner manufacturers, and heterogeneous image resolutions, enabling the automatic extraction of lesion morphometrics in large multi-site cohorts.
- Quantitative MRI biomarkers, namely, lesion length and maximal axial damage ratio derived from the automatic predictions showed no statistically significant difference when compared with manual ground truth, implying reliability in *SCIseg*'s predictions.

This work has been submitted to Radiology: Artificial Intelligence for possible publication. Copyright may be transferred without notice, after which this version may no longer be accessible.

Abstract

Purpose: To develop a deep learning tool for the automatic segmentation of T2-weighted intramedullary lesions in spinal cord injury (SCI).

Material and Methods: This retrospective study included a cohort of SCI patients from three sites enrolled between July 2002 and February 2023. A deep learning model, *SCIseg*, was trained in a three-phase process involving active learning for the automatic segmentation of intramedullary SCI lesions and the spinal cord. The data consisted of T2-weighted MRI acquired using different scanner manufacturers with heterogeneous image resolutions (isotropic/anisotropic), orientations (axial/sagittal), lesion etiologies (traumatic/ischemic/hemorrhagic) and lesions spread across the cervical, thoracic and lumbar spine. The segmentations from the proposed model were visually and quantitatively compared with other open-source baselines. Wilcoxon signed-rank test was used to compare quantitative MRI biomarkers (lesion volume, lesion length, and maximal axial damage ratio) computed from manual lesion masks and those obtained automatically with *SCIseg* predictions.

Results: MRI data from 191 SCI patients (mean age, 48.1 years \pm 17.9 [SD]; 142 males) were used for model training and evaluation. *SCIseg* achieved the best segmentation performance for both the cord and lesions. There was no statistically significant difference between lesion length and maximal axial damage ratio computed from manually annotated lesions and those obtained using *SCIseg*.

Conclusion: Automatic segmentation of intramedullary lesions commonly seen in SCI replaces the tedious manual annotation process and enables the extraction of relevant lesion morphometrics in large cohorts. The proposed model segments lesions across different etiologies, scanner manufacturers, and heterogeneous image resolutions. *SCIseg* is open-source and accessible through the Spinal Cord Toolbox.

Keywords

Spinal Cord, Trauma, Segmentation, MR-Imaging, Supervised learning, Convolution Neural Networks (CNN)

List of Abbreviations

DCM = degenerative cervical myelopathy

DL = deep learning

RVE = relative volume error

SC = spinal cord

SCI = spinal cord injury

SCT = Spinal Cord Toolbox

1. Introduction

Spinal cord injury (SCI) refers to damage to the spinal cord (SC) due to traumatic or non-traumatic processes. Traumatic SCI results from acute damage to the spinal cord (SC) due to external physical factors (1,2). The majority of traumatic SCI patients sustain permanent neurological deficits such as motor and autonomic dysfunction with devastating physical and social consequences (1). Degenerative cervical myelopathy (DCM), the most common form of non-traumatic SCI, originates from chronic mechanical compression of the spinal cord (3). While relatively less common than traumatic lesions, ischemic SCI lesions represent up to 20% of all non-traumatic lesions (4,5) and show a similar course of recovery to traumatic SCI (6,7). MRI provides macrostructural information about the level of injury, intramedullary abnormalities (e.g., edema and hemorrhage), and allows the evaluation of soft tissue structures (1,3). Importantly, MRI-derived quantitative biomarkers, namely, intramedullary lesion length and lesion volume, have demonstrated associations with the neurological prognosis of traumatic SCI patients (7–12).

Despite recent advances in automatic SC MRI processing (13–16), robust methods for automatic quantitative MRI biomarker identification in SCI are still missing. As a result, most studies involve manual identification of these biomarkers (7,11,17–20), which is a time-consuming process potentially susceptible to inter-rater variability across sites, making it less reproducible in multi-site studies (3). Furthermore, segmentation of intramedullary SCI lesions in MRI scans poses an extremely challenging task mainly due to the evolving appearance of lesions in different injury phases (e.g., acute, sub-acute, intermediate) (1,2). The surgical implants in postoperative MRI scans might also cause severe image artifacts. Deep learning (DL) can improve the diagnosis and prognostication in SCI by automating the lesion annotation process, thereby reducing rater-specific biases and facilitating the analysis of large SCI cohorts across sites (21–23). Indeed, quantitative SCI lesion biomarkers derived from DL-based automatic segmentations have been shown to correlate well with clinical measures of motor impairment (24). However, despite its numerous advantages, DL has not been sufficiently explored in the context of SCI (22), with no open-source methods existing to date. This suggests a need for an automatic biomarker identification method that deals with the complex pathophysiology of SCI patients, generalizes to multiple sites and is easily accessible by researchers.

Our objective was to develop an open-source DL-based tool, *SCIseg*, for the automatic segmentation of the spinal cord and intramedullary lesions from T2-weighted MRI scans of SCI patients [R1.10]. We evaluated two hypotheses: first, that quantitative MRI biomarkers derived automatically, such as lesion volume, lesion length, and maximal axial damage ratio, would not significantly differ from those identified manually. Second, we hypothesized that these biomarkers would correlate with clinical measures post-SCI. To this end, we conducted

correlation analyses between biomarkers derived using the automatic `SCIseg` and clinical scores, specifically pinprick, light touch, and lower extremity motor scores. [R1.9, R2.1]

2. Materials and Methods

2.1 Study Design and Participants

This retrospective study included a cohort of 191 SCI patients from three sites enrolled between July 2002 and February 2023. All patients provided written informed consent following Institutional Review Board approval and the Declaration of Helsinki. From site 1, 97 patients were enrolled out of which 61 had surgical hardware (dorsal/ventral spondylodesis), 13 underwent decompressive surgery, and the remaining 23 patients did not undergo surgery. From site 2, 80 patients were enrolled, all of which had post-operative metallic stabilization. Lastly, 14 patients were enrolled from site 3, out of which 8 had surgical hardware, 2 had decompressive surgery and 4 patients did not undergo any surgery. Details on patient demographics, injury levels, injury chronicity, scanner types, etc. can be found in Table 1. [AC, DE]. The inclusion criteria were: traumatic or ischemic SCI, patients with and without hardware, clinical MRI available for analyses, and completed enrollment. Exclusion criteria were: concurrent traumatic brain injury beyond concussion, and significant pre-existing neurological history (i.e., multiple sclerosis, transverse myelitis, cerebrovascular stroke). Patients from site 2 were clinically assessed using the international standards for the neurological classification of SCI (ISNCSCI) protocol (25) to obtain light touch, pinprick, and lower extremity motor scores as previously described in studies by Smith et al. (11,26). Patients from all sites were reported previously (7,11,17,26,27). These articles used manually annotated lesion masks to study the clinical consequences of SCI and their predictive relationships with motor and sensory functions. In contrast, our study presents a DL-based tool to automatically segment intramedullary SCI lesions.

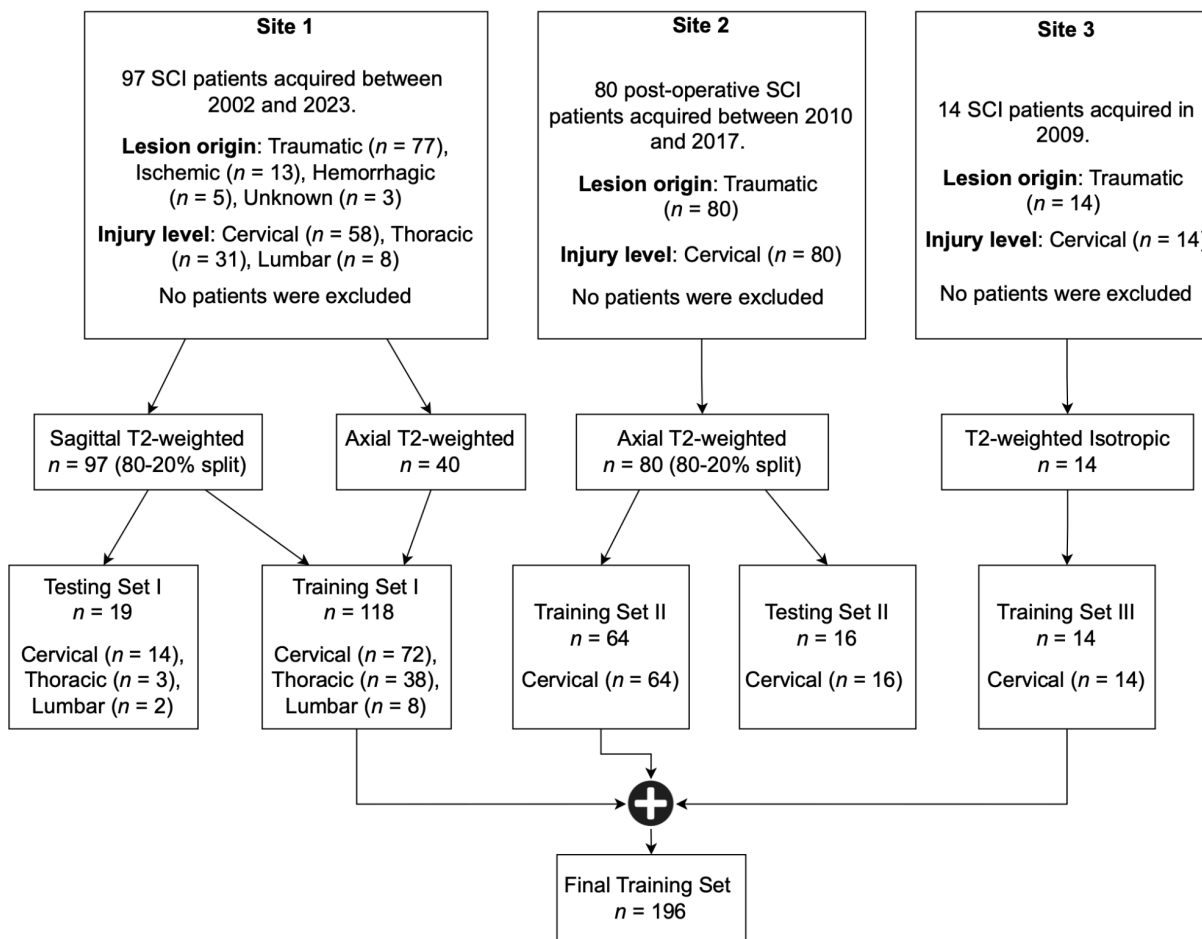


Figure 1: Study Flowchart. The data included patient cohorts from three sites with heterogeneous image resolutions, orientations, and lesion etiologies. The validation set is included within the final training set. Models were evaluated independently on the test sets of Site 1 and Site 2. Please refer to Table 1 for details on the MRI vendors and field strengths.

2.2 MRI Data

The MRI scans were converted from DICOM to NIfTI format and organized according to the BIDS standard (28) at individual sites. During this curation process, the scans were anonymized (i.e., all sensitive patient information was deleted). T2-weighted (T2w) MRI scans with varying lesion etiologies (traumatic, ischemic, hemorrhagic), injury chronicity (sub-acute, intermediate, and chronic), orientations (sagittal/axial), and voxel sizes were used for this study (Figure 1, Table 1). Lesions appearing as T2w signal abnormalities (hyperintense or hypointense voxels corresponding to primary contusions, secondary cytotoxic edema or hemorrhage [R1.13, R1.14]) were manually annotated as a single object by two raters from site 1, one rater from site 2, and one rater from site 3 using JIM and FSLeves image viewers. As obtaining the ground truth (GT) SC segmentation masks using a fully manual approach is time-consuming,

`sct_deepseg_sc` (29) was used to initially segment the SC for all 3 sites, followed by manual corrections wherever necessary. Such semi-automatic approaches were also reported in previous studies (29,30). [R1.21, R2.6]

2.3 Deep Learning Training Protocol

The model was trained in three phases (Figure 2). In the initial phase, a baseline segmentation model was trained using a labelled dataset of 78 subjects with T2-weighted sagittal scans (site 1) and 64 subjects with T2-weighted axial scans (site 2). We used the *region-based training* strategy of nnUNet (31), where the model initially segments the SC and then localizes itself on the SC to segment the T2-weighted lesions subsequently. The lesions are segmented as a single object covering hyperintense and hypointense voxels hence containing both edema and hemorrhage. [R1.14, R1.25] Default data augmentation methods by nnUNet were used, namely, random rotation, scaling, mirroring, Gaussian noise addition, Gaussian blurring, adjusting image brightness and contrast, low-resolution simulation, and Gamma transformation. All scans were preprocessed with RPI orientation and Z-score normalization. The model was trained for 1000 epochs, with a batch size of 2 using the stochastic gradient descent optimizer with a polynomial learning rate scheduler.

For the second phase, we used the human-in-the-loop active learning strategy (32) to gradually include axial T2-weighted scans from site 1 in the training dataset. Using the phase 1 baseline model, we generated initial SC and lesion predictions for unlabeled axial scans from site 1. A subset of predicted segmentations underwent quality control, with two raters manually correcting if needed. These refined segmentations were then added to the training dataset, resulting in the inclusion of 40 scans and leading to a total of 182 scans in the training set.

To further improve our model's generalization capabilities to a wide range of image resolutions, we added a new dataset from site 3 containing 14 *isotropic* T2-weighted sagittal scans of traumatic SCI patients in the third training phase. In summary, the final dataset consisting of 196 scans gathered from three sites was used for training the model with the region-based strategy described above.

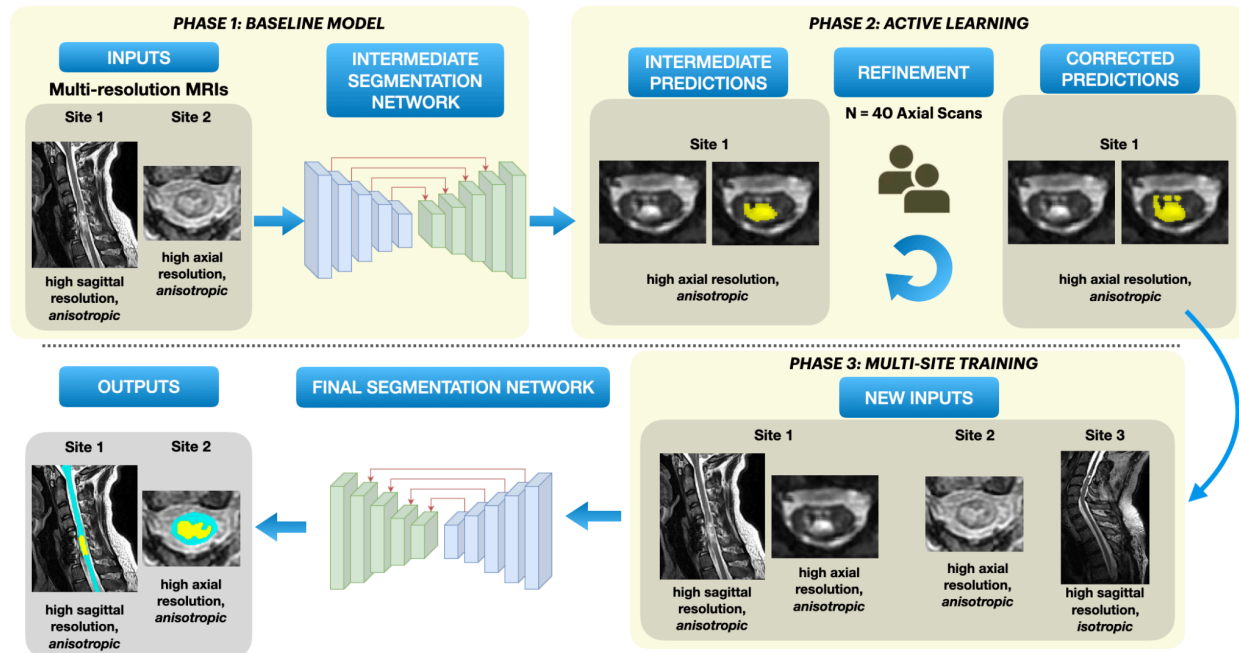


Figure 2: Overview of our segmentation approach. Phase 1: A baseline model is trained on data consisting of T2-weighted scans with axial and sagittal orientations from two sites. Phase 2: *Active learning* – Initial batch of automatic predictions on T2-weighted axial scans from site 2 are obtained, followed by manual corrections. Phase 3: Along with the newly corrected axial scans, isotropic T2-weighted sagittal scans from site 3 are added to the original dataset for multi-site training. The final model is trained to segment both spinal cord and lesion simultaneously.

2.4 Evaluation Protocol

We created two independent test sets (site 1: $n=19$, site 2: $n=16$), following the 80/20 train/test splitting ratio (Table 1). To ensure an unbiased assessment of the model's performance and avoid overfitting, the train/test splits were done at the patient-level (and not at the image-level), ensuring that sagittal and axial scans of a particular patient strictly belonged only to the training or testing set. [R1.12, R1.16] We trained five models, each with a different train/test splitting using a different random seed, to avoid biasing the model towards a particular dataset split. The model's performance on the lesion and SC segmentation were evaluated independently within each test set by comparing it with open-source methods available in Spinal Cord Toolbox (SCT) (15): `sct_propseg` (33), `sct_deepseg_sc` (29), and the recently proposed `contrast-agnostic` SC segmentation model (30). Due to the lack of existing state-of-the-art, open-source methods for SCI lesion segmentation, we compared the `SCIseg` 3D model with its 2D version. Additionally, we tested our model on an independent cohort of 14 DCM patients from site 1 (unseen during training) to evaluate its generalization on non-traumatic SCI patients.

2.5 Evaluation Metrics

For quantitative validation, we used the segmentation metrics from the open-source ANIMA toolkit (<https://anima.readthedocs.io/en/latest/index.html>). For SC segmentation, we presented the Dice coefficient and the relative volume error (RVE). For lesion segmentation, we reported the Dice coefficient, average surface distance, lesion-wise positive predictive value (PPV), lesion-wise sensitivity, and F_1 score (34). As we trained five models on five random train/test splits, some patients were present in more than one test set. We thus averaged the metrics across test splits for such patients.

2.6 Quantitative MRI Biomarkers

We used the SCT's `sct_analyze_lesion` function to automatically compute the total lesion volume, intramedullary lesion length, and maximal axial damage ratio (11) from the manual ground-truth lesion masks and the automatic predictions using the proposed `SCIseg 3D` model. To assess the effect of adding more training data during active learning, we computed the quantitative MRI biomarkers before (phase 1) and after active learning (phase 3). The quantitative MRI biomarkers were then averaged across five random test splits. Additionally, for site 2, we correlated the quantitative MRI biomarkers with the clinical scores (light touch, pinprick, and lower extremity motor scores).

2.7 Statistical Analysis

Statistical analysis was performed using the SciPy Python library v1.11.4 (35). Data normality was tested using D'Agostino and Pearson's normality test. Between-group comparisons (lesion segmentation performance `SCIseg 2D` vs. `SCIseg 3D`; `SCIseg` lesion segmentation performance before (phase 1) vs. after active learning (phase 3); manual lesion GT vs. `SCIseg`-predicted lesions) were performed using the Wilcoxon signed-rank test. Correlations between clinical scores and quantitative MRI biomarkers were examined using the Spearman rank-order correlation.

3. Results

3.1 Patient Characteristics

A total of 191 patients (mean age \pm standard deviation 48.1 ± 17.9 , 142 males, 42 females, 7 sex not reported) with 231 MRI scans from three sites with different lesion etiologies (traumatic/ischemic/hemorrhagic) were included in this study (Figure 1, Table 1). Eight patients from site 1 were followed up with additional MRI examinations. Patients were scanned across scanners from different manufacturers (Siemens, Philips, GE) with different field strengths (1T,

1.5T, 3T). T2-weighted scans used in this study had heterogeneous image resolutions, and orientations (Table 1).

Table 1: Characteristics of the Study Cohort

	Site 1	Site 2	Site 3
Number of patients	97	80	14
Number of MRI scans	137[R1.29] [†]	80	14
Sex (male/female)	66/25*	65/15	11/2
Age (mean ± standard deviation)	51.0 ± 19.1	45.8 ± 16.4	42.9 ± 16.7
Age range	17–83	15–81	21–65
Days from injury to MRI (mean ± standard deviation)	376.2 ± 1364.4 [‡]	84.0 ± 212.1	579.1 ± 714.1
Days from injury to MRI (median)	41.5	21.0	407
Number of patients with surgical implants/hardware	61 3T (n=19), 1.5T (n=41), 1T (n=1)	80 3T (n=21), 1.5T (n=59)	8 3T (n=10)
Lesion origin [R1.13, R1.14, R3.4]	Traumatic (n=77) Ischemic (n=13) Hemorrhagic (n=5) Unknown origin (n=3)	Traumatic (n=80)	Traumatic (n=14)
Injury level [R3.2, R3.6]	Cervical (n=58) Thoracic (n=31) Lumbar (n=8)	Cervical (n=80)	Cervical (n=14)
Number of patients in train set	Cervical (n=44) Thoracic (n=28) Lumbar (n=6) Total (n=78)	Cervical (n=64)	Cervical (n=14)
Number of patients in test set	Cervical (n=14) Thoracic (n=3) Lumbar (n=2) Total (n=19)	Cervical (n=16)	0
MRI manufacturers	Siemens (n=91), GE (n=5), Philips (n=1)	Siemens (n=20), GE (n=60)	Siemens (n=14)

MRI field strength	3T (n=37), 1.5T (n=59), 1T (n=1)	3T (n=21), 1.5T (n=59)	3T (n=14)
MRI Sequence parameters	SAGITTAL T2-weighted: voxel size 0.34 × 0.34 mm to 0.96 × 0.96 mm; slice thickness 2.2 mm to 4.8 mm	AXIAL T2-weighted: voxel size 0.31 × 0.31mm to 0.78 × 0.78mm; slice thickness from 3.0 mm to 6.0 mm	ISOTROPIC T2-weighted: voxel size 0.84 × 0.84 × 0.94 mm to 0.875 × 0.875 × 0.9mm
	AXIAL T2-weighted: voxel size 0.35 × 0.35 mm to 0.78 × 0.78 mm; slice thickness 1.0 mm to 7.0 mm		

*Sex not reported for 7 patients

†Eight patients were followed up with more than 1 MRI examination

‡Five scans were acquired very late after injury resulting in high average time for MRI examination

3.2 Automatic Spinal Cord and Lesion Segmentation in SCI

Table 2 shows the quantitative results of *SCIseg* 3D on test sets of the two sites. We observed that SC segmentations from the model are quite stable across different data splits despite the presence of artifacts in the scans. However, for lesion segmentation, the model showed better performance on site 2 compared to site 1 with a high standard deviation across splits.

Table 2. Quantitative performance of the proposed *SCIseg* 3D model. The metrics are averaged across 5 random seeds.

Metric	Spinal Cord Segmentation		
	Site 1 (n=79)	Site 2 (n=51)	Average (n=130)
Dice Score (↑)	0.90 ± 0.08	0.94 ± 0.04	0.92 ± 0.07
RVE % (↓)	0.25 ± 15.19	0.51 ± 10.33	0.35 ± 13.45
Surface Distance (↓)	0.14 ± 0.66	0.00 ± 0.00	0.09 ± 0.52
	Lesion Segmentation		
Dice Score (↑)	0.51 ± 0.30	0.74 ± 0.15	0.61 ± 0.27
Surface Distance (↓)	3.51 ± 9.61	0.30 ± 1.34	2.17 ± 7.54

Lesion-wise PPV (\uparrow)	0.53 ± 0.43	0.88 ± 0.26	0.67 ± 0.41
Lesion-wise Sensitivity (\uparrow)	0.79 ± 0.36	0.91 ± 0.22	0.84 ± 0.32
F ₁ Score (\uparrow)	0.55 ± 0.43	0.86 ± 0.24	0.68 ± 0.39

Note: Data are means \pm standard deviations. The best value for surface distance and RVE is 0.0 and 1.0 for the rest of the metrics.

3.3 Comparison with Other Methods

We compared the SC segmentation performance of our `SCIseg 3D` model with other methods: `sct_propseg`, `sct_deepseg_sc 2D`, `sct_deepseg_sc 3D`, `contrast-agnostic`, and `SCIseg 2D` (Figure 3, Figure 4). The half-violin plots in Figure 4 show the distribution of the Dice scores and RVE for test scans across all seeds and the scatter plots show the performance of the models on each test scan.

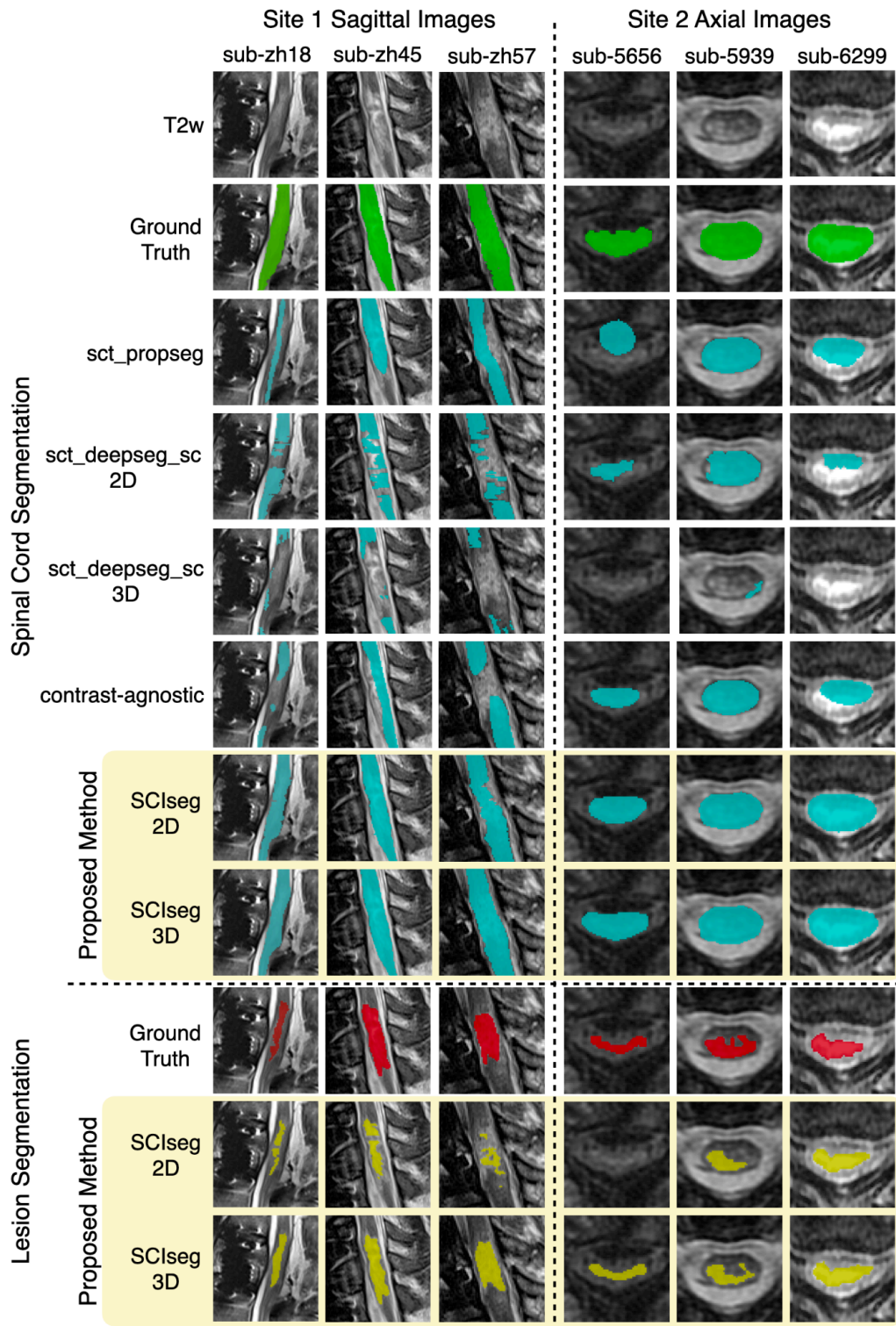


Figure 3: Comparison of *SCIseg* with baseline methods for the spinal cord and lesion segmentation on patients from site 1 and site 2. Notice that *SCIseg* 3D provides the best results qualitatively for both spinal cord and lesion segmentation at the site of lesions.

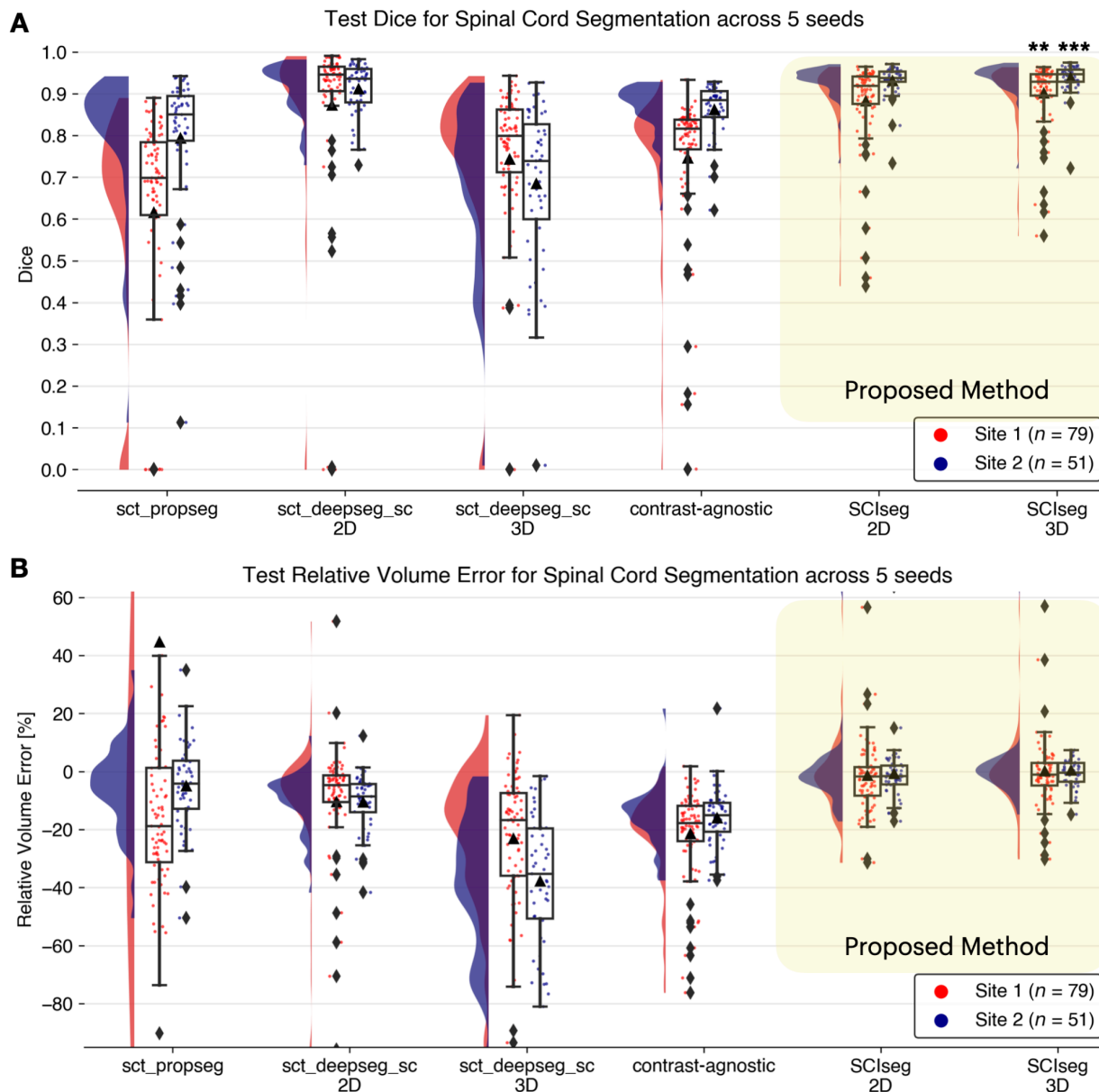


Figure 4: Raincloud plots comparing the (A) Dice scores (best: 1; worst: 0) and (B) relative volume error (in %, best: 0%) across various spinal cord segmentation methods. The numbers in the legend represent the number of test scans in each site across 5 different training seeds. Notice that although the `sct_deepseg_sc 2D` and `SClseg 3D` have similar Dice scores, the former shows a higher under-segmentation (negative relative volume error) compared to the latter. *** $P < .05$ (two-sided Bonferroni-corrected pairwise Wilcoxon signed-rank test for `SClseg 3D` with all baselines), ** $P < .001$ (statistically significant for all pairs except `SClseg 3D` and `sct_deepseg_sc 2D`).

3.3.1 Spinal Cord Segmentation

Our model, *SCIseg 3D*, achieves the best segmentation performance across all baselines (Figure 4). For site 1, *SCIseg 3D* model outputs SC segmentations for all test cases including those where the baselines output empty predictions (shown by diamonds at Dice=0 in Figure 4A). We also observed more under-/over-segmented predictions for site 1 (shown by a larger spread of scatter points around RVE=0% in Figure 4B). On visual quality control of such cases, we noticed that the scans contained substantial metal implants, interfering with our model's ability to fully segment the SC. On the other hand, for site 2, our model performed robustly across all test scans. Figure 4A shows that the distribution of Dice scores for one of the baseline models (*sct_deepseg_sc 2D*) is similar to *SCIseg 3D*. As described in Section 2.2, this is the consequence of the fact that the semi-automatic approach involving *sct_deepseg_sc 2D* was used to create the GT SC masks. As a result, quantitative evaluations involving the GT masks obtained from this baseline model are inherently biased to be higher than the rest of the methods in comparison. Lastly, it must be noted that all baselines were trained specifically for segmenting the spinal cord, whereas the proposed *SCIseg 3D* model can segment both SC and lesions simultaneously.

3.3.2 Lesion Segmentation

Table 3 presents a comparison between the 2D and 3D variants of the *SCIseg* model. The 3D model performs significantly better than the 2D model across all metrics for both sites. As for the performance within sites, the model's performance on site 2 is higher than that of site 1. Through visual quality control, we noticed that site 1 contained several patients with metal implants causing heavy image artifacts and patients spanned different SCI phases (acute and sub-acute) with various degrees of lesion hyperintensity, thus making automatic segmentation challenging. Despite these issues, the *SCIseg* model provides a good starting point for obtaining lesion segmentations instead of manually annotating lesions from scratch.

Table 3. Lesion segmentation performance of the *SCIseg* models. The metrics are averaged across 5 different training seeds.

Metric	SCIseg 2D		SCIseg 3D	
	Site 1 (n=79)	Site 2 (n=51)	Site 1 (n=79)	Site 2 (n=51)
Dice Score (\uparrow)	0.36 \pm 0.31	0.65 \pm 0.21	0.51 \pm 0.30[†]	0.74 \pm 0.15[†]
Surface Distance (\downarrow)	9.14 \pm 32.43	0.54 \pm 1.48	3.51 \pm 9.61[‡]	0.30 \pm 1.34[†]
Lesion-wise PPV (\uparrow)	0.33 \pm 0.43	0.73 \pm 0.35	0.53 \pm 0.43[†]	0.88 \pm 0.26[‡]

Lesion-wise Sensitivity (\uparrow)	0.63 ± 0.46	0.89 ± 0.27	0.79 ± 0.36 [†]	0.91 ± 0.22
F ₁ Score (\uparrow)	0.35 ± 0.43	0.74 ± 0.33	0.55 ± 0.43 [†]	0.86 ± 0.24 [‡]

Note: Data are means \pm standard deviations. The best value for surface distance is 0.0 and 1.0 for the rest of the metrics. Bold represents better performance.

[†] Statistically significant compared to *SCIseg* 2D. Wilcoxon signed-rank test ($P < .001$)

[‡] Statistically significant compared to *SCIseg* 2D. Wilcoxon signed-rank test ($P < .05$)

3.4 Effect of Active Learning on Lesion Segmentation

We performed an ablation study comparing the model performance after phase 1 (training on 2 sites) and phase 3 (training on 3 sites after active learning). Figure 5A shows the correlation between manual ground truth and automatic predictions for total lesion volume (top) and intramedullary lesion length (bottom). For both sites, a higher agreement between the manually annotated and automatically derived lesion metrics can be observed for the final model after the third phase of training (i.e., solid lines moving closer to the diagonal identity line). The improvement after active learning (phase 3) was statistically significant (Wilcoxon signed-rank test, $p < 0.05$) in estimating the total lesion volume for both sites and only the lesion length for site 1.

Figure 5B shows the performance of our baseline model after phase 1 of training (before active learning) on unseen axial T2-weighted scans from site 1. The model tends to under-segment the lesions. However, we noticed an overall improvement in the segmentations when trained on more data consisting of axial scans from site 1 and isotropic sagittal scans from site 3 during phase 3 of training.

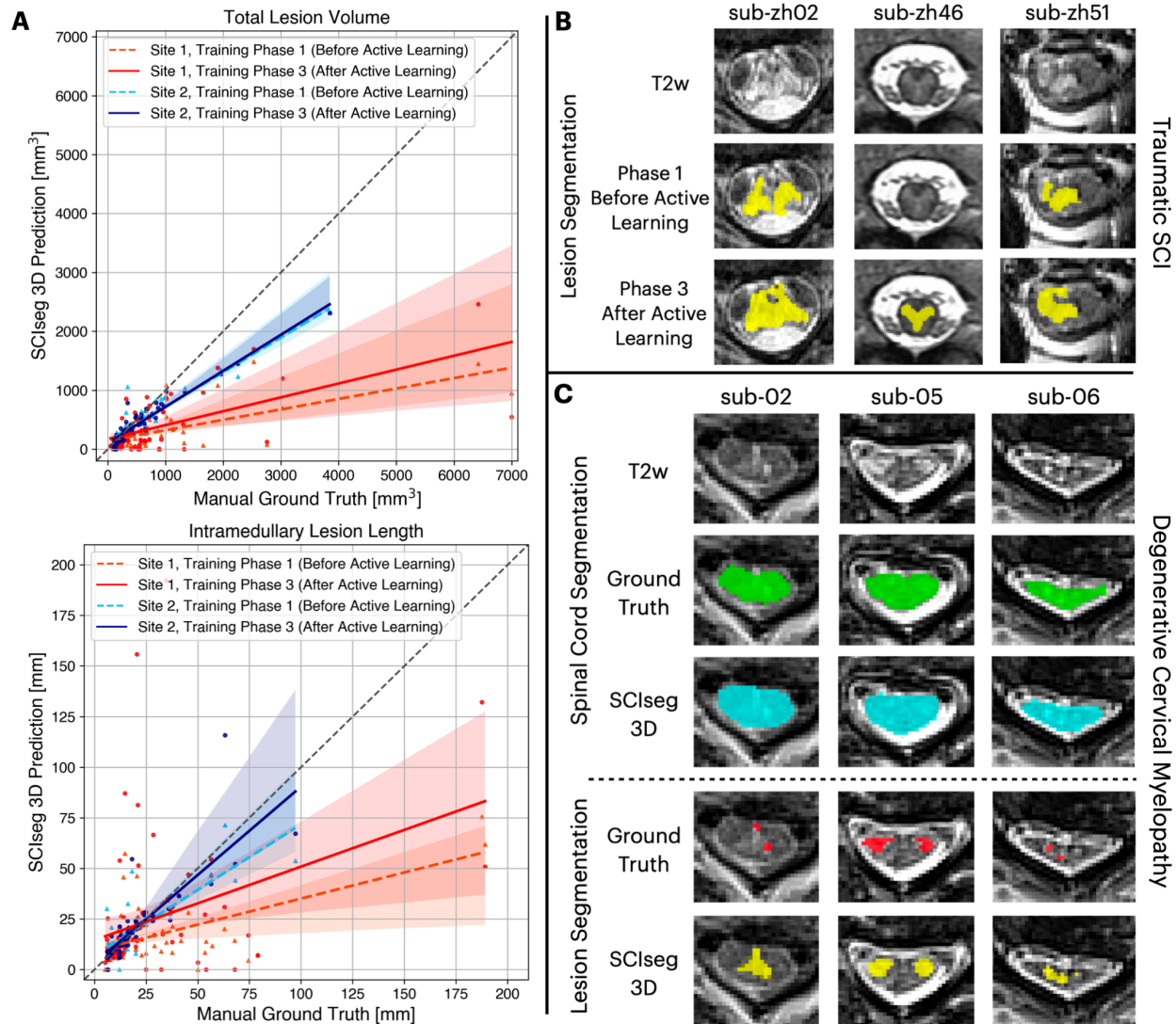


Figure 5: Comparison of model performance before and after active learning. (A) Correlation plots for total lesion volume (top) and intramedullary lesion length (bottom) computed from manual ground truth (GT) lesion masks (x-axis) and lesion predictions from the proposed SCIseg 3D model (y-axis). Within each plot, coloured dashed and solid lines show the agreement between manual GT and automatic predictions before and after active learning, respectively, site 1 (red/orange) and site 2 (blue/light-blue). Note that the model's predictions after active learning show a higher agreement with the manual GT for both sites (i.e., solid lines move closer to the diagonal identity line). (B) SCIseg's predictions on unseen axial images from site 2 before and after active learning. (C) Examples of SCIseg's generalization to non-traumatic SCI (i.e., degenerative cervical myelopathy, DCM) patients. Notice that the model obtains an accurate SC segmentation even at the level of severe compression (sub-06).

3.5 Generalization to Degenerative Cervical Myelopathy

Qualitative examples of SC and lesion segmentation on an independent cohort of DCM patients unseen during training are shown in Figure 5C. Interestingly, in cases where the ground-truth lesion masks were under-segmented, the model provided a better and more complete segmentation of the lesion. Furthermore, the SC segmentations are accurate even for slices with severe SC compression (Figure 5C, *sub-06*). For quantitative validation, we also computed the Dice and F_1 scores for both SC and lesion segmentations (Table 4).

Table 4. Quantitative evaluation of *SCIseg 3D* model's generalization to non-traumatic SCI (i.e., DCM) patients. The metrics are averaged across 5 random seeds.

Metric	Spinal Cord Segmentation
Dice Score (\uparrow)	0.95 \pm 0.01
RVE % (\downarrow)	3.51 \pm 4.63
Surface Distance (\downarrow)	0.00 \pm 0.00
Lesion Segmentation	
Dice Score (\uparrow)	0.46 \pm 0.26
Surface Distance (\downarrow)	1.51 \pm 4.64
Lesion-wise PPV (\uparrow)	0.71 \pm 0.38
Lesion-wise Sensitivity (\uparrow)	0.50 \pm 0.45
F_1 Score (\uparrow)	0.49 \pm 0.44

Note: Data are means \pm standard deviations. The best value for surface distance and RVE is 0.0 and 1.0 for the rest of the metrics.

3.6 Correlation between Clinical Scores and MRI Biomarkers

Figure 6 illustrates the relationship between clinical scores (specifically, pinprick, light touch, and lower extremity motor scores) and quantitative MRI biomarkers (namely, lesion volume, lesion length, and maximal axial damage ratio) calculated from both manual ground-truth lesion masks and lesions predicted using *SCIseg 3D*. We observed statistically significant correlations ($P < .05$) between the clinical scores and lesion biomarkers (Figure 6). The Wilcoxon signed-rank test between manual (yellow) vs. *SCIseg*-predicted (green) lesion

biomarkers revealed no statistically significant ($P > .05$) difference for lesion length and maximal axial damage ratio, while lesion volume showed a significant difference ($P < .05$).

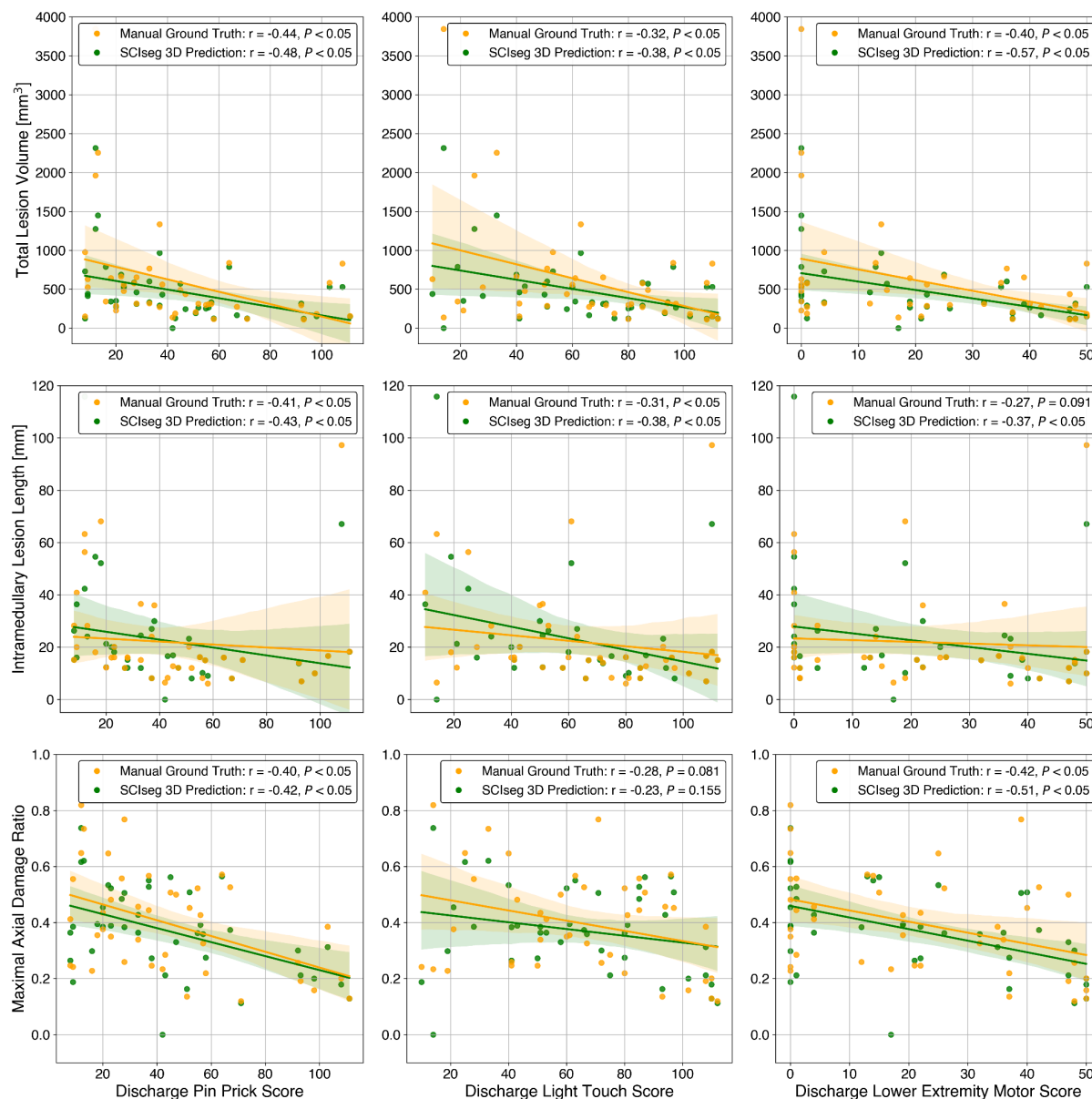


Figure 6: Correlation analysis between discharge clinical scores (x-axis) and quantitative MRI biomarkers (y-axis) for site 2. Spearman correlation coefficient and p-value are shown in the legends. The Wilcoxon signed-rank test between manual ground-truth lesion masks (yellow) vs. automatic predictions using SCIsseg 3D (green) lesion biomarkers revealed no statistically significant ($P > .05$) difference for lesion length and maximal axial damage ratio, while lesion volume showed a significant difference ($P < .05$).

4. Discussion

This study introduced a DL-based model, *SCIseg*, for the automatic segmentation of the spinal cord and intramedullary lesions in SCI patients from T2-weighted MRI scans. The model was trained and evaluated on a cohort of 191 traumatic and non-traumatic SCI patients with 231 scans acquired using different scanner manufacturers with heterogeneous image resolutions (isotropic/anisotropic), orientations (axial/sagittal), lesion etiologies (traumatic/ischemic/hemorrhagic) and lesions spread across the cervical, thoracic and lumbar spine. To the best of our knowledge, *SCIseg* is the first open-source, automatic method for lesion and spinal cord segmentation in SCI. It also generalizes to DCM patients, producing accurate segmentations for both lesions and SC at the compression levels.

As the segmentation performance might be constrained by the low data quality and small dataset sizes in SCI, we showed that implementing a three-phase training strategy, including an active learning approach to progressively expand the dataset size and incorporating diverse data distributions into the training set, contributes significantly towards enhancing the model performance. Furthermore, a region-based training strategy that jointly segments the SC and the lesion is more efficient than training two individual models for SC and lesion segmentation, respectively. As a result, correlation analyses between clinical scores and MRI-derived biomarkers showed statistically significant relationships ($P < .05$) for both manually annotated ground truth and automatically derived lesion masks, suggesting the *SCIseg* predictions can be reliably used for correlation with clinical measures in SCI.

Our cohort predominantly consisted of traumatic SCI lesions in intermediate and chronic phases as the prevalence of ischemic and hemorrhagic lesions is typically lower (4). As chronic injuries tend to be more delineated on T2w scans (2), our model learned to be sensitive to hyperintense abnormalities in the image. This also explains its ability to segment DCM lesions which also tend to be hyperintense at the site of compression. Similarly, as the injury levels in the training dataset were skewed towards the cervical spine, its ability to segment lumbar lesions is expected to be lower compared to cervical/thoracic lesions. [R3.2, R3.8]

Only a few studies exist in the literature discussing the importance of automatic segmentation in SCI scans (24,36). McCoy et al.'s study (24) is the closest to ours as it presented the first DL method for the segmentation of SC and intramedullary lesions in SCI. Nevertheless, there are several important distinctions between the two studies. While their model was trained on axial scans of pre-operative (acute) SCI patients from a single site, our model was trained on multi-site data consisting of traumatic and ischemic SCI patients with different image orientations (axial/sagittal). Moreover, our model was exposed to more heterogeneous data covering different injury chronicities (intermediate/chronic) and therefore demonstrated better generalization to both traumatic and non-traumatic lesion etiologies. More importantly, our work is open-source, further enabling reproducible, multi-site studies in SCI.

This study has a few limitations. First, longitudinal scans from patients with follow-up examinations were treated as independent inputs for training. While the lesion appearance evolved between sessions, resulting in non-identical lesions (hence justifying our choice of treating them as independent inputs), the model was unlikely to learn the evolution of lesions across time. Second, the model's sensitivity to hyperintense abnormalities might result in false positive segmentations in healthy controls where the SC central canal is visualized. Third, our limited training set size of 196 scans risks overfitting, given the complexity of the SCI lesion segmentation task. While we gathered diverse data from 3 sites and trained 5 models with different train/test splits along with extensive data augmentation to prevent potential overfitting, increasing the dataset size would further improve the model's performance and generalization. Lastly, we did not analyze the inter-rater variability as the data were gathered from multiple sites and there were no overlapping subjects across sites. Previous studies (37,38) have reported that MRI measures of spinal cord damage (e.g., edema length, midsagittal tissue bridge ratio, axial damage ratio) exhibit high-to-excellent levels of inter-rater reliability.

There exist several promising avenues for future work. The segmentation models can be improved by using more fine-grained ground-truth masks, where the hyperintense edema and hypointense hemorrhage could be treated as separate classes. Training a model on pre-operative traumatic SCI data using these ground-truth masks would have a major impact on improving the initial classification of the disease and further prognostication (18). While the model generalizes reasonably well to DCM lesions, there is a scope for improvement, especially, by adding the DCM cohort to the existing training set or by training a DL model exclusively on DCM data. Previous studies have reported the presence of hyperintense T2-weighted lesions in up to 64% of DCM patients (13,39,40) and explored the relationship between structural and functional damages (41). Such studies would greatly benefit from an automatic DCM lesion segmentation method.

In conclusion, this study presented *SCIseg*, an automatic DL-based method for the segmentation of SC and intramedullary lesions in SCI from T2-weighted MRI scans. The work has addressed several limitations of previous studies, first, a large retrospective cohort consisting of 191 patients spanning three sites was used, second, MRI data was acquired using scanners from different manufacturers, and third, a single model was trained to segment *both* SC and lesions. More importantly, the methodology has been designed to ensure reproducibility and enable large-scale, reproducible prospective studies. The model is open-source and accessible via SCT (v6.2 and higher). We hope that *SCIseg* will benefit clinicians and patients by providing additional diagnostic and prognostic information, serving as a basis for further studies assessing optimal rehabilitation from a customized patient-based perspective.

Code Availability Statement

To facilitate reproducibility and open science principles, all codes, processing scripts, and results are shared as open-source and freely available to the whole community at https://github.com/ivadomed/model_seg_sci.

Acknowledgements

We thank Nick Guenther and Mathieu Guay-Paquet for their assistance with the management of the datasets, Joshua Newton for his contributions in helping us implement the algorithm to SCT, Maxime Bouthillier for his help in correcting parts of the manuscript, Drs. Thierry Albert, Bertrand Baussart, Caroline Hugeron, Hugues Pascal Moussellard, Frédéric Petit and Marc-Antoine Rousseau for helping with patient recruitment in Paris, Dr. Serge Rossignol and the Multidisciplinary Team on Locomotor Rehabilitation (Regenerative Medicine and Nanomedicine, CIHR), and we thank all patients.

Funding

Funded by the Canada Research Chair in Quantitative Magnetic Resonance Imaging [CRC-2020-00179], the Canadian Institute of Health Research [PJT-190258], the Canada Foundation for Innovation [32454, 34824], the Fonds de Recherche du Québec - Santé [322736, 324636], the Natural Sciences and Engineering Research Council of Canada [RGPIN-2019-07244], the Canada First Research Excellence Fund (IVADO and TransMedTech), the Courtois NeuroMod project, the Quebec BiImaging Network [5886, 35450], INSPIRED (Spinal Research, UK; Wings for Life, Austria; Craig H. Neilsen Foundation, USA), Mila - Tech Transfer Funding Program, the Association Française contre les Myopathies (AFM), the Institut pour la Recherche sur la Moelle épinière et l'Encéphale (IRME), the National Institutes of Health Eunice Kennedy Shriver National Institute of Child Health and Development (R03HD094577). ACS is supported by the National Institutes of Health – K01HD106928 and R01NS128478 and the Boettcher Foundation's Webb-Waring Biomedical Research Program. KAW is supported by the National Institutes of Health – K23NS104211, L30NS108301, R01NS128478. JV received funding from the European Union's Horizon Europe research and innovation programme under the Marie Skłodowska-Curie grant agreement No 101107932 and is supported by the Ministry of Health of the Czech Republic, grant nr. NU22-04-00024. ENK is supported by the Fonds de Recherche du Québec Nature and Technologie (FRQNT) Doctoral Training Scholarship and in part by the FRQNT Strategic Clusters Program (2020-RS4-265502 - Centre UNIQUE - Union Neurosciences & Artificial Intelligence – Quebec and in part, by funding from the Canada First Research Excellence Fund through the TransMedTech Institute. The authors thank Digital Research Alliance of Canada for the compute resources used in this work.

References

1. Ahuja CS, Wilson JR, Nori S, et al. Traumatic spinal cord injury. *Nat Rev Dis Primers*. 2017;3:17018. doi: 10.1038/nrdp.2017.18.
2. Freund P, Seif M, Weiskopf N, et al. MRI in traumatic spinal cord injury: from clinical assessment to neuroimaging biomarkers. *Lancet Neurol*. 2019;18(12):1123–1135. doi: 10.1016/S1474-4422(19)30138-3.
3. David G, Mohammadi S, Martin AR, et al. Traumatic and nontraumatic spinal cord injury: pathological insights from neuroimaging. *Nat Rev Neurol*. 2019;15(12):718–731. doi: 10.1038/s41582-019-0270-5.
4. Scivoletto G, Torre M, Mammone A, et al. Acute Traumatic and Ischemic Spinal Cord Injuries Have a Comparable Course of Recovery. *Neurorehabil Neural Repair*. 2020;34(8):723–732. doi: 10.1177/1545968320939569.
5. New PW, Cripps RA, Bonne Lee B. Global maps of non-traumatic spinal cord injury epidemiology: towards a living data repository. *Spinal Cord*. 2014;52(2):97–109. doi: 10.1038/sc.2012.165.
6. Iseli E, Cavigelli A, Dietz V, Curt A. Prognosis and recovery in ischaemic and traumatic spinal cord injury: clinical and electrophysiological evaluation. *J Neurol Neurosurg Psychiatry*. 1999;67(5):567–571. doi: 10.1136/jnnp.67.5.567.
7. Pfyffer D, Huber E, Sutter R, Curt A, Freund P. Tissue bridges predict recovery after traumatic and ischemic thoracic spinal cord injury. *Neurology*. 2019;93(16):e1550–e1560. doi: 10.1212/WNL.00000000000008318.
8. Miyanji F, Furlan JC, Aarabi B, Arnold PM, Fehlings MG. Acute cervical traumatic spinal cord injury: MR imaging findings correlated with neurologic outcome--prospective study with 100 consecutive patients. *Radiology*. Radiological Society of North America (RSNA); 2007;243(3):820–827. doi: 10.1148/radiol.2433060583.
9. Dobran M, Aiudi D, Liverotti V, et al. Prognostic MRI parameters in acute traumatic cervical spinal cord injury. *Eur Spine J*. 2023;32(5):1584–1590. doi: 10.1007/s00586-023-07560-4.
10. Huber E, Lachappelle P, Sutter R, Curt A, Freund P. Are midsagittal tissue bridges predictive of outcome after cervical spinal cord injury? *Ann Neurol*. 2017;81(5):740–748. doi: 10.1002/ana.24932.
11. Smith AC, Albin SR, O'Dell DR, et al. Axial MRI biomarkers of spinal cord damage to predict future walking and motor function: a retrospective study. *Spinal Cord*. 2021;59(6):693–699. doi: 10.1038/s41393-020-00561-w.
12. Kurpad S, Martin AR, Tetreault LA, et al. Impact of Baseline Magnetic Resonance Imaging on Neurologic, Functional, and Safety Outcomes in Patients With Acute Traumatic Spinal Cord Injury. *Global Spine Journal*. SAGE Publications; 2017;7(3 Suppl):151S. doi:

10.1177/2192568217703666.

13. Martin AR, De Leener B, Cohen-Adad J, et al. A novel MRI biomarker of spinal cord white matter injury: T2*-weighted white matter to gray matter signal intensity ratio. *AJNR Am J Neuroradiol*. 2017;38(6):1266–1273. doi: 10.3174/ajnr.A5162.
14. Badhiwala JH, Ahuja CS, Akbar MA, et al. Degenerative cervical myelopathy - update and future directions. *Nat Rev Neurol*. 2020;16(2):108–124. doi: 10.1038/s41582-019-0303-0.
15. De Leener B, Lévy S, Dupont SM, et al. SCT: Spinal Cord Toolbox, an open-source software for processing spinal cord MRI data. *Neuroimage*. 2017;145(Pt A):24–43. doi: 10.1016/j.neuroimage.2016.10.009.
16. Bischof A, Papinutto N, Keshavan A, et al. Spinal Cord Atrophy Predicts Progressive Disease in Relapsing Multiple Sclerosis. *Ann Neurol*. 2022;91(2):268–281. doi: 10.1002/ana.26281.
17. Smith AC, Weber KA 2nd, O'Dell DR, Parrish TB, Wasielewski M, Elliott JM. Lateral Corticospinal Tract Damage Correlates With Motor Output in Incomplete Spinal Cord Injury. *Arch Phys Med Rehabil*. 2018;99(4):660–666. doi: 10.1016/j.apmr.2017.10.002.
18. Mummaneni N, Burke JF, DiGiorgio AM, et al. Injury volume extracted from MRI predicts neurologic outcome in acute spinal cord injury: A prospective TRACK-SCI pilot study. *J Clin Neurosci*. *J Clin Neurosci*; 2020;82(Pt B):231–236. doi: 10.1016/J.JOCN.2020.11.003.
19. Vallotton K, Huber E, Sutter R, Curt A, Hupp M, Freund P. Width and neurophysiologic properties of tissue bridges predict recovery after cervical injury. *Neurology*. 2019;92(24):e2793–e2802. doi: 10.1212/WNL.0000000000007642.
20. Pfyffer D, Vallotton K, Curt A, Freund P. Predictive Value of Midsagittal Tissue Bridges on Functional Recovery After Spinal Cord Injury. *Neurorehabil Neural Repair*. 2021;35(1):33–43. doi: 10.1177/1545968320971787.
21. Khan O, Badhiwala JH, Wilson JRF, Jiang F, Martin AR, Fehlings MG. Predictive Modeling of Outcomes After Traumatic and Nontraumatic Spinal Cord Injury Using Machine Learning: Review of Current Progress and Future Directions. *Neurospine*. 2019;16(4):678–685. doi: 10.14245/ns.1938390.195.
22. Dietz N, Vaitheesh Jaganathan, Alkin V, Mettillie J, Boakye M, Drazin D. Machine learning in clinical diagnosis, prognostication, and management of acute traumatic spinal cord injury (SCI): A systematic review. *J Clin Orthop Trauma*. 2022;35:102046. doi: 10.1016/j.jcot.2022.102046.
23. Asgari Taghanaki S, Abhishek K, Cohen JP, Cohen-Adad J, Hamarneh G. Deep semantic segmentation of natural and medical images: a review. *Artificial Intelligence Review*. 2021;54(1):137–178. doi: 10.1007/s10462-020-09854-1.
24. McCoy DB, Dupont SM, Gros C, et al. Convolutional Neural Network-Based Automated

- Segmentation of the Spinal Cord and Contusion Injury: Deep Learning Biomarker Correlates of Motor Impairment in Acute Spinal Cord Injury. *AJNR Am J Neuroradiol.* 2019;40(4):737–744. doi: 10.3174/ajnr.A6020.
25. Rupp R, Biering-Sørensen F, Burns SP, et al. International Standards for Neurological Classification of Spinal Cord Injury: Revised 2019. *Top Spinal Cord Inj Rehabil.* 2021;27(2):1–22. doi: 10.46292/sci2702-1.
 26. Smith AC, O'Dell DR, Thornton WA, et al. Spinal Cord Tissue Bridges Validation Study: Predictive Relationships With Sensory Scores Following Cervical Spinal Cord Injury. *Top Spinal Cord Inj Rehabil.* 2022;28(2):111–115. doi: 10.46292/sci21-00018.
 27. Cohen-Adad J, El Mendili MM, Lehericy S, et al. Demyelination and degeneration in the injured human spinal cord detected with diffusion and magnetization transfer MRI. *Neuroimage.* Elsevier Inc.; 2011;55(3):1024–1033. doi: 10.1016/j.neuroimage.2010.11.089.
 28. Gorgolewski KJ, Auer T, Calhoun VD, et al. The brain imaging data structure, a format for organizing and describing outputs of neuroimaging experiments. *Scientific Data.* Dordrecht: Springer Netherlands; 2016;3(1):160044. doi: 10.1038/sdata.2016.44.
 29. Gros C, De Leener B, Badji A, et al. Automatic segmentation of the spinal cord and intramedullary multiple sclerosis lesions with convolutional neural networks. *Neuroimage.* 2019;184:901–915. doi: 10.1016/j.neuroimage.2018.09.081.
 30. Bédard S, Enamundram NK, Tsagkas C, et al. Towards contrast-agnostic soft segmentation of the spinal cord. *arXiv [eess.IV].* 2023. <http://arxiv.org/abs/2310.15402>.
 31. Isensee F, Jaeger PF, Kohl SAA, Petersen J, Maier-Hein KH. nnU-Net: a self-configuring method for deep learning-based biomedical image segmentation. *Nat Methods.* 2021;18(2):203–211. doi: 10.1038/s41592-020-01008-z.
 32. Budd S, Robinson EC, Kainz B. A survey on active learning and human-in-the-loop deep learning for medical image analysis. *Med Image Anal.* 2021;71:102062. doi: 10.1016/j.media.2021.102062.
 33. De Leener B, Kadoury S, Cohen-Adad J. Robust, accurate and fast automatic segmentation of the spinal cord. *Neuroimage.* 2014; doi: 10.1016/j.neuroimage.2014.04.051.
 34. Commowick O, Istace A, Kain M, et al. Objective Evaluation of Multiple Sclerosis Lesion Segmentation using a Data Management and Processing Infrastructure. *Sci Rep.* 2018;8(1):13650. doi: 10.1038/s41598-018-31911-7.
 35. Virtanen P, Gommers R, Oliphant TE, et al. SciPy 1.0: fundamental algorithms for scientific computing in Python. *Nat Methods.* Nature Publishing Group; 2020;17(3):261–272. doi: 10.1038/s41592-019-0686-2.
 36. Blanc C, Shahrapour S, Mohamed FB, de Leener B. Combining PropSeg and a

convolutional neural network for automatic spinal cord segmentation in pediatric populations and patients with spinal cord injury. *Int J Imaging Syst Technol*. John Wiley & Sons, Ltd; 2023;n/a(n/a). doi: 10.1002/ima.22859.

37. Smith AC, Weber KA, Parrish TB, et al. Ambulatory function in motor incomplete spinal cord injury: a magnetic resonance imaging study of spinal cord edema and lower extremity muscle morphometry. *Spinal Cord*. 2017;55(7):672–678. doi: 10.1038/sc.2017.18.
38. Cummins DP, Connor JR, Heller KA, et al. Establishing the inter-rater reliability of spinal cord damage manual measurement using magnetic resonance imaging. *Spinal Cord Ser Cases*. 2019;5:20. doi: 10.1038/s41394-019-0164-1.
39. Nouri A, Martin AR, Kato S, Reihani-Kermani H, Riehm LE, Fehlings MG. The Relationship between MRI Signal Intensity Changes, Clinical Presentation, and Surgical Outcome in Degenerative Cervical Myelopathy. *Spine* . 2017;42(24):1851–1858. doi: 10.1097/BRS.0000000000002234.
40. Martin AR, Tadokoro N, Tetreault L, et al. Imaging Evaluation of Degenerative Cervical Myelopathy: Current State of the Art and Future Directions. *Neurosurgery Clinics of North America*. *Neurosurg Clin N Am*; 2018. p. 33–45. doi: 10.1016/j.nec.2017.09.003.
41. Scheuren PS, David G, Kipling Kramer JL, et al. Combined Neurophysiologic and Neuroimaging Approach to Reveal the Structure-Function Paradox in Cervical Myelopathy. *Neurology*. 2021; doi: 10.1212/WNL.0000000000012643.